Acoustic impedance interpretation for hydrocarbon extent, offshore Brunei Darussalam

S. Ronghe[1] & P. V. Trung[2]

Introduction

Interpretation on acoustic impedance volumes – the product of 3D seismic inverse modelling – has considerable advantages compared to conventional seismic data interpretation. Acoustic impedance data images layers as opposed to interfaces imaged on seismic data. Hence interpretations can be made on lithological units rather than on their boundaries, and extracted properties relate to rock layers rather than interfaces. Acoustic impedance sections feature improvements in layer visualization and vertical resolution (Duboz *et al.* 1998; Latimer *et al.* 2000). In addition, acoustic impedance can serve as a direct hydrocarbon indicator (Ruijtenberg *et al.* 1990), and can be correlated with other petrophysical parameters – such as porosity – that characterize a reservoir (Brown 1996; Burge & Neff 1998). Hence the decomposition of a seismic data volume into an acoustic impedance volume through seismic inverse modelling can be important, not only for facilitating direct interpretation of the reservoir layer, but also for characterizing reservoir quality through the subsequent derivation of petrophysical parameters, and for possibly mapping the extents of hydrocarbon saturation.

This study performed seismic inverse modelling and interpretation of the acoustic impedance volume to decipher the vertical and lateral limits of gas saturation in two sands in a field currently under development. The two sands, separated by about 350 m, were chosen for their contrasting characters (Table 1): a shallower Sand 1 strongly defined on seismic data, having higher average thickness, porosity and gas saturation at well locations; and a poorer quality Sand 2 with lower average gas saturation, not as clearly defined on seismic data, occurring at about the start of overpressured depths. Hence this research aimed to study the effectiveness and limitations of seismic inverse modelling and acoustic impedance interpretation on two reservoir sands having markedly differing characteristics.

[1] Department of Petroleum Geoscience, Universiti Brunei Darussalam, Jalan Tungku Link, Negara Brunei Darussalam BE 1410.

[2] PetroVietnam Exploration and Production, Block G1, Thanh Da Hotel, Ward 27, Binh Thanh District, Ho Chi Minh City, Vietnam.

Geological setting

The field is situated 45 km offshore Brunei Darussalam (Fig. 1) in the Baram Delta Province of Neogene age. The stratigraphic succession is a northward prograding regressive sequence deposited in a series of cycles separated by marine transgressive phases (James 1984; Sandal 1996). The two sand units of interest are of Early Pliocene age and are interpreted as delta front or upper shoreface deposits. The structural development of the offshore Baram Delta Province was influenced by syn-sedimentary tectonics related to rapid and abundant sedimentation. The field is situated within a regional basin-hading growth fault zone and is associated with a prominent NE-SW trending regional growth fault (F1). All hydrocarbon bearing blocks occur on the hanging wall side of this growth fault, dip to the north, and are separated by normal faults.

The data set comprised 64 sq km areal coverage of 3D seismic data at line and trace spacing of 25 m, along with wireline logs from five wells. Figure 2 illustrates the gamma ray and sonic log correlations of the two sands. The tops of the sands have sharp contacts, while their basal transitions are gradational. The sands generally have higher velocities than the surrounding shales. The thickness of the interval defined by the two sands is approximately constant. The overall fining upward structure of the gamma ray log reflects the geological model of a single regressive deltaic depositional sequence. The good correlation of these and other sands between the wells suggests deposition as widespread sheets.

Synthetic seismograms

Well to seismic correlation was undertaken by means of a synthetic seismogram constructed at each well location. The construction of a synthetic seismogram requires, firstly, the transformation of wireline logs from depth to time domain, and secondly, the extraction of an accurate source wavelet. Checkshots at each well were used to transform wireline logs and well markers from depth mode into two-way travel time equivalent. A wavelet was determined at each well as a least squares inverse filter which, when convolved with the reflectivity series, generates the closest possible synthetic trace ap-

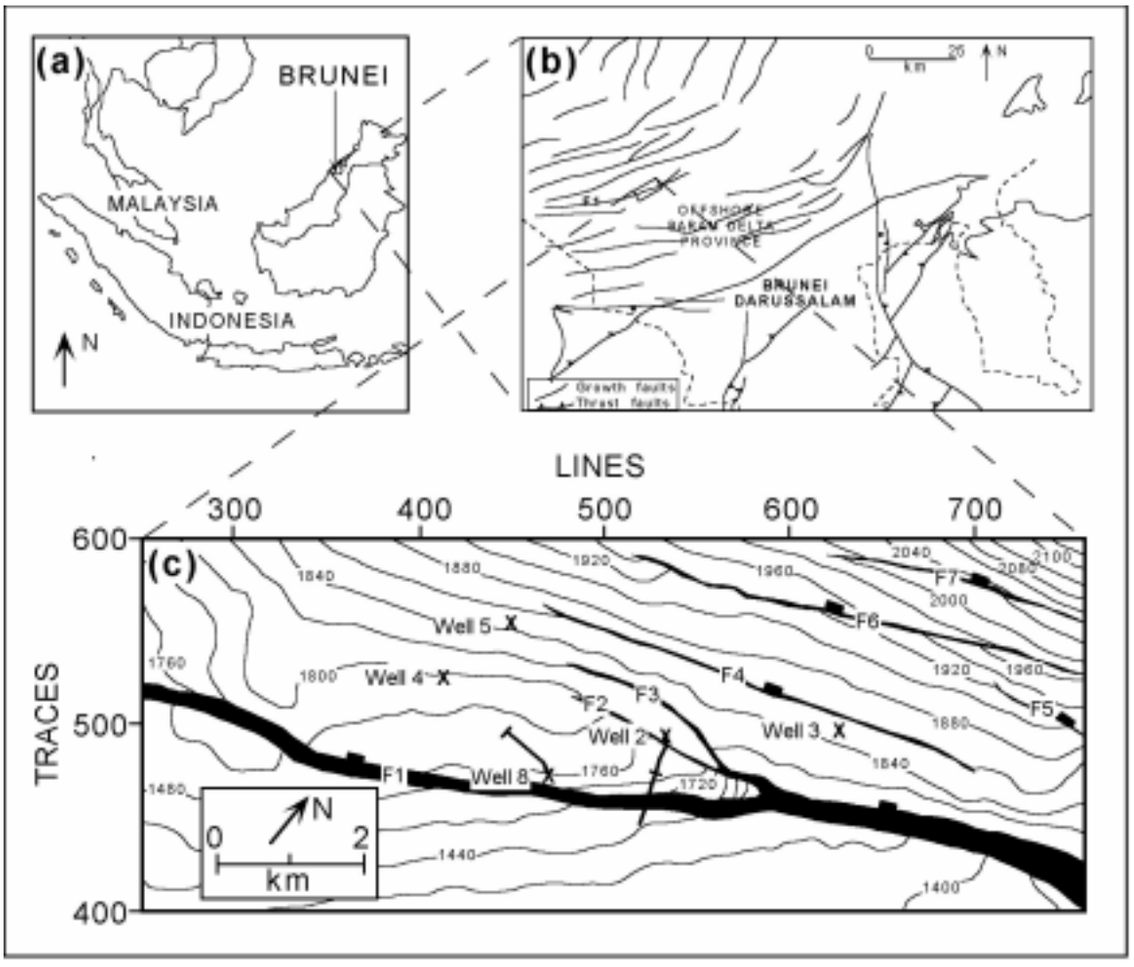

Figure 1 Geological setting of the study area. (a) Regional location. (b) Structural trends of Brunei Darussalam (modified from James 1984). (c) Time structure map of the Sand 1 horizon. Contour intervals are 20 ms. F1 to F7 are faults. Well downhole positions marked by 'X'. Well trajectory indicated by line. Intersection location of well Sand 1 marker with interpreted time structure horizon indicated by tick along well trajectory.

Table 1 Sand unit characteristics obtained from wireline data.

Sand unit (m TVD)	Depth range (m)	Ave. thickness (%)	Ave. porosity	Ave. gas saturation (%)
Sand 1	1921–2096	18	27	80
Sand 2	2261–2340	11	12	54

proximation to the seismic trace. The five wavelets were averaged into a single wavelet (Fig. 3) representative of this data set. In retrospect, the wavelet could have been shortened or further tapered to reduce or eliminate the ringing above 30 Hz in the amplitude spectrum.

Figures 4 and 5 illustrate wireline logs, a synthetic seismogram and a synthetic-seismic overlay for two wells (4 and 3). Note that Gardner's relationship between sonic and density was used to recreate these logs where missing in the data set. Both figures show a good visual match between the synthetic and seismic data and this is corroborated by their fairly high synthetic-seismic cross-correlation coefficients (0.548 and 0.623, respectively). The tuning thickness for the interval of interest calculated using the dominant wavelet frequency (12 Hz) and average wireline velocity (3100 m/s) is about 64 m. Both Sand 1 and Sand 2 have thickness less than tuning thickness. Consequently, neither is able to generate independent seismic responses from their upper and lower boundaries. The seismic events associated with Sand 1 have high amplitudes that are laterally well defined across the data set. In contrast, Sand 2 generates weak events that are laterally discontinuous. The poorer response of Sand 2 may be a

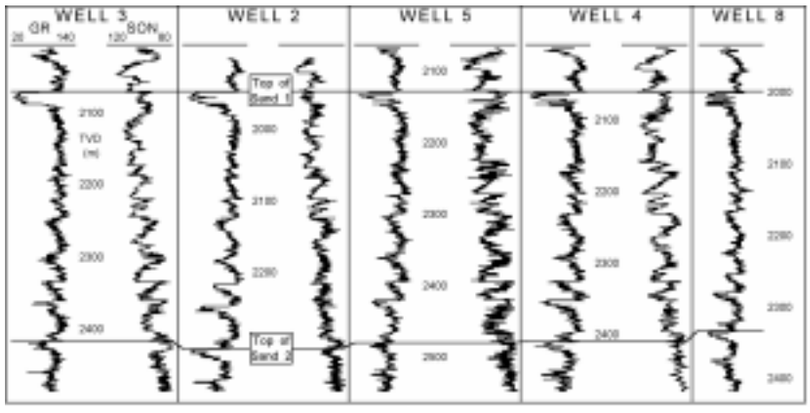

Figure 2 Gamma ray and sonic log correlations for the two sands.

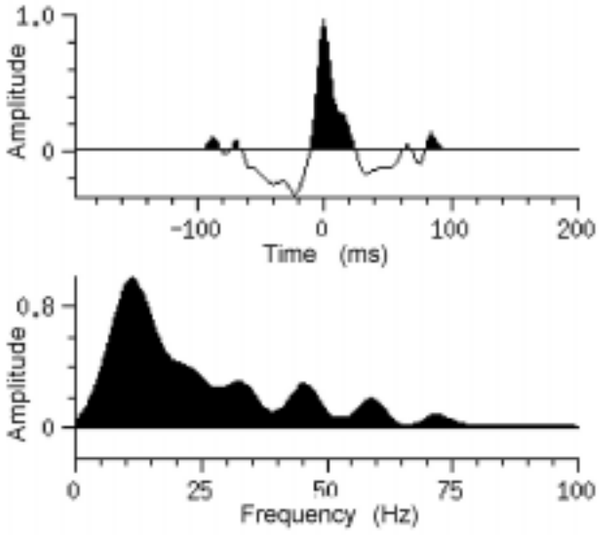

Figure 3 Estimated representative wavelet characteristics.

consequence of the combined effects of its lower thickness, petrophysical differences influenced by its deeper stratigraphic level (explained further later), and destructive wavelet interference from overlying strata including an immediately overlying sand unit.

The synthetic seismograms demonstrate, most prominently for Sand 1, polarity reversals between the water-bearing and hydrocarbon-bearing sections. In Well 4, the positive value of reflection coefficient at the upper boundary of the water-bearing Sand 1 (Table 2) creates a relatively strong peak on the synthetic and seismic traces. In Well 3, Sand 1 is gas saturated. Consequently, acoustic impedance is lowered, the reflection coefficient for its upper boundary is transformed into a negative value and correlates with a strong trough event on the synthetic and seismic traces. This switch of reflection coefficient from positive to negative values is also apparent in Table 2 for the upper boundary of Sand 2 between its water-bearing section (Well 3) and gas-saturated section (Well 4). However, the poor expression of Sand 2

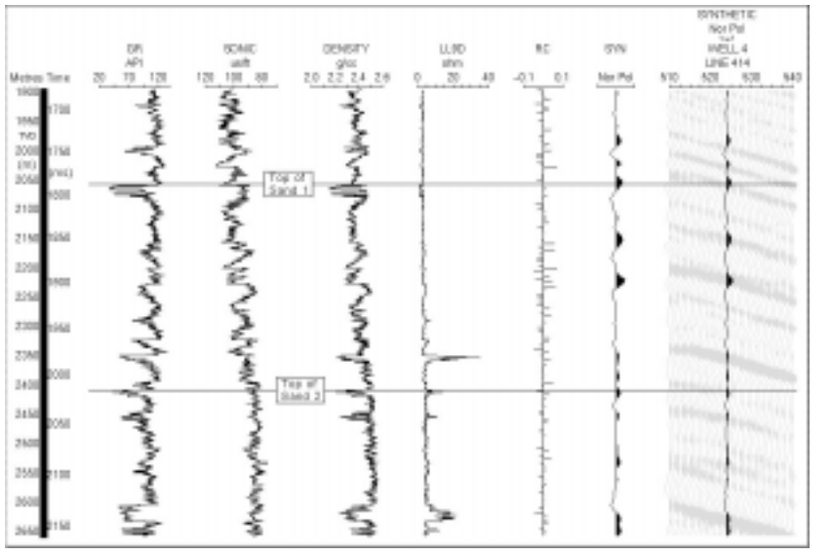

Figure 4 Well 4: wireline logs, synthetic seismogram, and synthetic-seismic overlay.

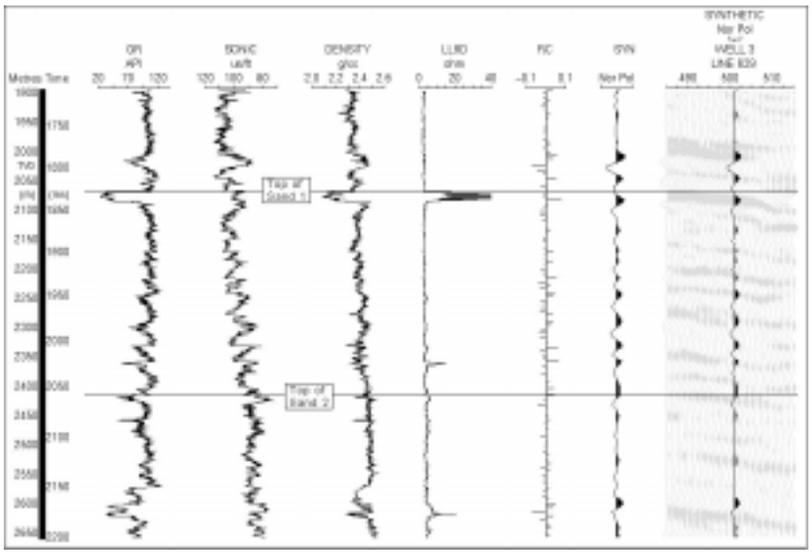

Figure 5 Well 3: wireline logs, synthetic seismogram, and synthetic-seismic overlay.

Table 2 Boundary reflection coefficient values and fluid content of the two sands at each well location.

		Well 2		Well 3		Well 4		Well 5		Well 8	
Unit	Boundary	RC	Fluid	RC	Fluid	RC	Fluid	RC	Fluid	RC	Fluid
Sand 1	Top	– 0.08	Gas	– 0.01	Gas	0.01	Water	0.07	Water	– 0.08	Gas
	Base	0.10		0.03		– 0.04		– 0.08		0.08	
Sand 2	Top	– 0.10	Gas	0.05	Water	– 0.07	Gas	0.02	Water	– 0.08	Gas
	Base	0.09		– 0.08		0.07		– 0.04		0.08	

masks this polarity reversal on the synthetic and seismic data. For both Sand 1 and 2, waveform peaks were mapped over the study area. These correspond with the tops of the sands in their water bearing regions, and with the base of the sands in their gas saturated areas.

Wireline analysis

Figures 6 and 7 illustrate gamma ray vs. acoustic impedance crossplots from a 50-m interval distributed about each sand. The two wells used in each figure represent the different fluid types (gas or water) in the sands: a well where the sand is gas saturated (Well 2 for both sands) and a well where the sand is water filled (Well 4 for Sand 1 and Well 3 for Sand 2). In both figures, high values of GR (> 80 API) separate out the shales from the sands. Note that the shales and the water filled sands are indistinguishable in acoustic impedance, whereas gas saturated sands exhibit markedly lower impedances. This enables arbitrary acoustic impedance cut-off values to be set for each sand indicative of gas saturation. For Sand 1, impedances lower than about 6550 g/cc × m/s relate to the occurrence of hydrocarbon. The impedance cut-off of about 7800 g/cc × m/s for Sand 2, applied to Well 3, causes a substantial proportion of shale data samples to fall below this threshold. An explanation may be that these samples represent soft (water filled) shales at the deeper stratigraphic level of Sand 2. This explanation is strengthened by sonic logs in Figs 4 and 5 which suggest that Sand 2 occurs at about the start of overpressured depths. Sand 2 marks the location of a change in the sonic log trend. Below this, formation velocities do not show a progressive increase with depth. These considerations imply that acoustic impedance may be used as an indicator of hydrocarbon at the level of Sand 1; at the deeper level of Sand 2 such interpretations are likely to be ambiguous, since low acoustic impedances may be indicative either of hydrocarbon or of soft shale in the formation.

Inverse modelling

Seismic inverse modelling was performed using a 'model based' or 'blocky' algorithm. Sonic logs from the five wells and the two mapped horizons were used to build initial velocity and impedance models over the data volume. For each seismic trace, a synthetic seismogram was calculated using the impedance model and the averaged extracted wavelet. The impedance model was then modified gradually until the resulting synthetic traces matched the seismic traces within a pre-set tolerance level (25% permissible variation). Duboz

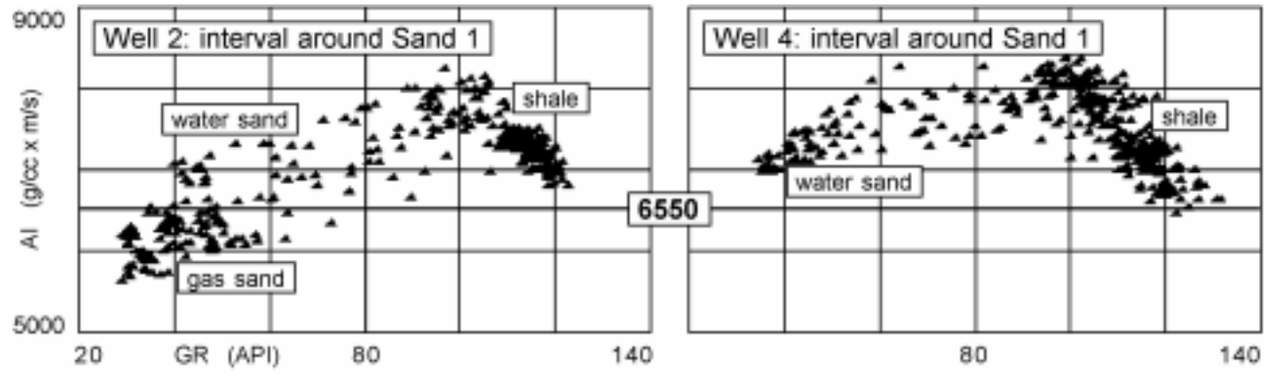

Figure 6 Sand 1: gamma ray vs. acoustic impedance crossplots from wells 2 and 4.

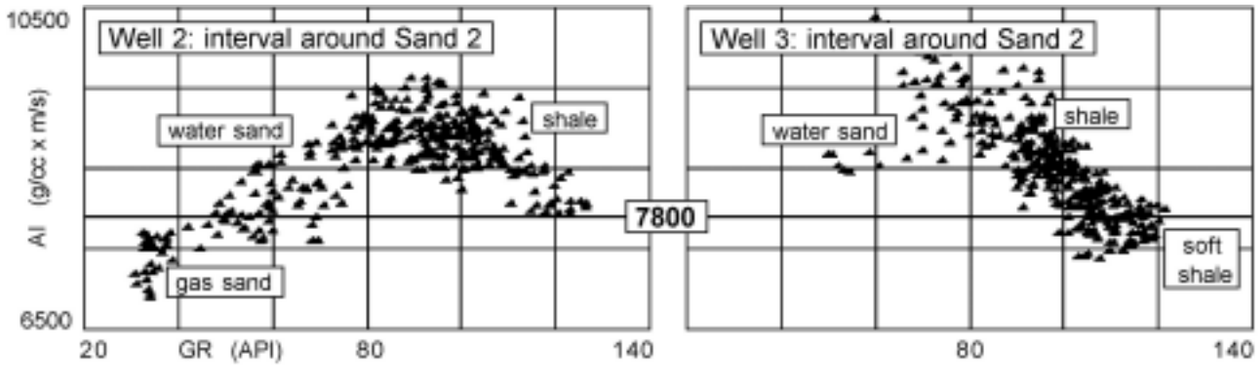

Figure 7 Sand 2: gamma ray vs. acoustic impedance crossplots from wells 2 and 3.

et al. (1998) state that such model based inversion methods have the advantage of better resolution over trace based inversion methods by attenuating random noise and reducing thin bed interference effects.

Figure 8 shows the resulting modelled impedance sections around each sand. Impedances at well location agree with modelled impedances, especially for the two sands, and testify to the accuracy of the parameters chosen as input into the modelling process, as well as provide confidence in the interpretation of impedance variations away from the wells. Interpretation on these AI sections allowed the delineation of the vertical boundaries of the gas saturated portions along with the determination of the downdip extent of the limit of gas saturation in each sand.

The map view distributions of minimum acoustic impedance extracted using a 20 ms window centred about each sand are illustrated in Fig. 9. For Sand 1, an area of low impedances occurs prominently in the structurally shallower area of the strata downthrown along fault F1, its northern limit defined by fault F4. This area of impedances lower than the established threshold of 6550 g/cc × m/s is indicative of the extent of gas saturation in the sand. The established cutoff allows for the delineation of the gas–water contact on the base map. Within this region of low impedances are three distinct locations where the extracted impedances are at their lowest (of about 4800 g/cc × m/s). These areas are interpreted as representing conditions of better reservoir quality (higher inferred porosities and lower clay content) leading to possibly higher hydrocarbon saturation. Other less significant areas of gas saturated Sand 1 are indicated by impedances slightly lower than the established threshold in the also structurally shallower western area of the map and in some downthrown sections of faults F4, F6 and F7. Isolated locations of impedances lower than threshold may represent pockets of residual gas captured in small stratigraphic traps during migration.

For Sand 2, low impedance anomalies cover the central, structurally shallow area of the map downthrown along fault F1, along with substantial portions of the north-east. The lithological and fluid classifications of impedance from wireline crossplot analysis have indicated that for Sand 2, impedances below the established threshold of 7800 g/cc × m/s may relate to both hydrocarbon occurrence as well as the presence of soft shale in the formation. The central area of low impedances is presumed to be indicative of gas saturation. This interpretation is substantiated by the fact that at wells 2, 4 and 8 occurring within this low impedance area,

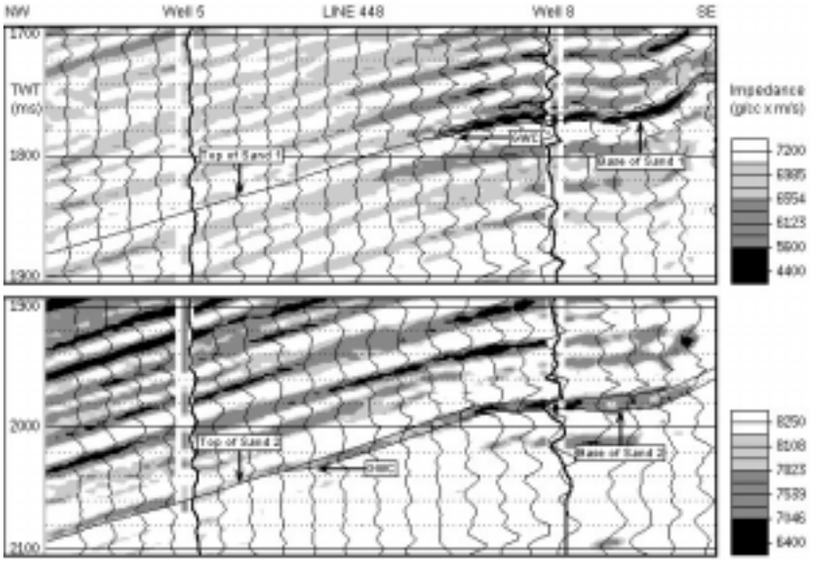

Figure 8 Derived acoustic impedance sections interpreted separately for each sand. See Fig. 1 for line location.

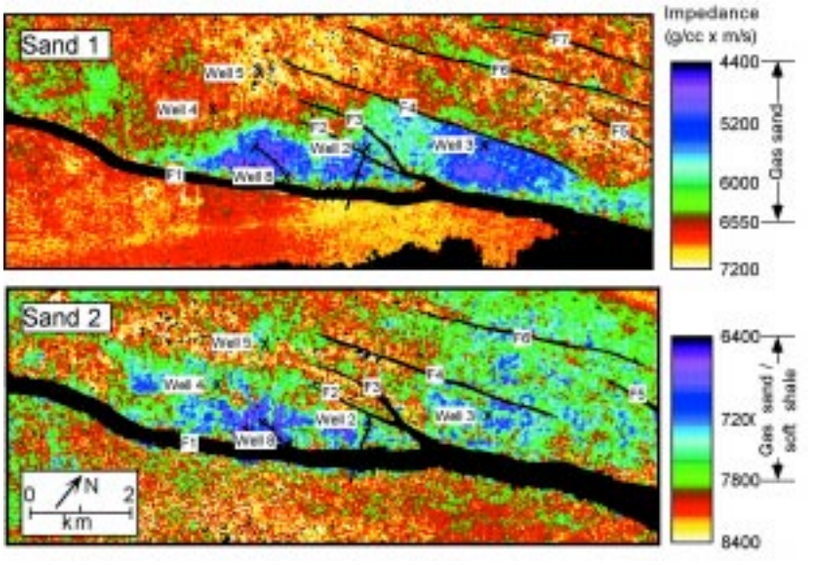

Figure 9 Extracted impedance maps for Sand 1 and Sand 2. Symbols as in Fig. 1.

Sand 2 is known to contain hydrocarbon from wireline log analysis. The threshold impedance marks the gas-water contact on the map. The low impedances to the north-east could be an influence of both hydrocarbon occurrence, as well as soft shale in the surrounding formation. Wireline analysis indicates that in Well 3 Sand 2 is water filled, and this suggests that the low impedances to the north-east are likely to be representative of soft shale.

Net pay estimation

Interpretation on acoustic impedance sections enabled the top and base of the gas saturated portions of each sand to be mapped separately. These horizons were converted to depth using the velocity model used in inversion modelling generated from wireline information. The depth converted horizons were then subtracted and contoured to obtain the isopach map of net pay distribution, illustrated in Fig. 10, for each sand. For Sand 1, net pay could be calculated over the area bounded by faults F1 and F4, whereas for Sand 2, interpretation uncertainties restricted calculation to the central portion of the field between faults F1 and F2. Figure 11 compares net pay estimated from acoustic impedance interpretation with the true (wireline measured) net pay. The similarity between estimated and true values attests towards the accuracy of this acoustic impedance interpretation for net pay calculation.

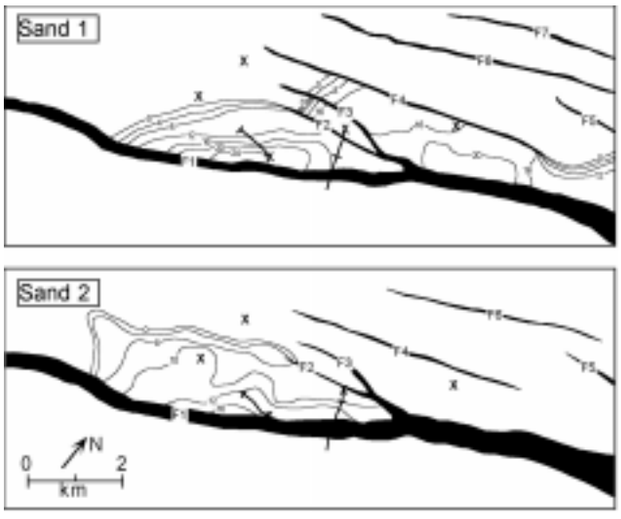

Figure 10 Extracted net pay distribution maps for Sand 1 and Sand 2. Contour values in meters. Symbols as in Fig. 1.

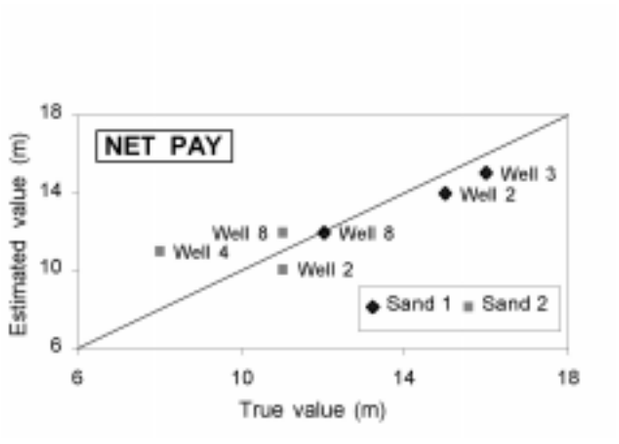

Figure 11 Crossplot of estimated net pay from impedance vs. true (wireline measured) net pay for Sand 1 and Sand 2.

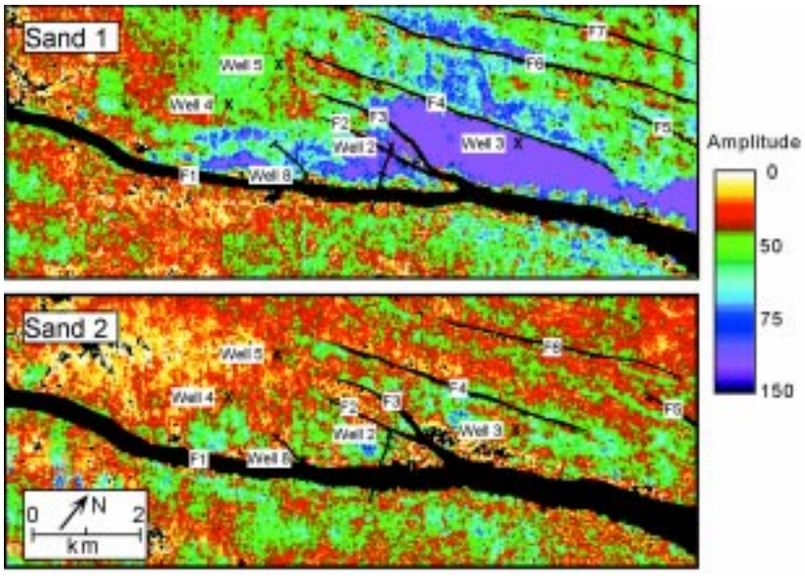

Figure 12 Extracted maximum peak amplitude maps for Sand 1 and Sand 2. Symbols as in Fig. 1.

Discussion and conclusion

The reflection coefficient characteristics of each sand (Table 2) correlated against fluid content suggest that this seismic dataset will respond in two ways to the occurrence of hydrocarbon: firstly, through an increase in amplitude; and secondly, through a reversal of polarity. The possibility of identifying the areal extent of hydrocarbon accumulation in each sand using amplitude and polarity characteristics are tested in Figs 12 and 13, respectively. Maximum peak amplitudes were extracted using a 20-ms window centred about the interpreted seismic horizon for each sand (Fig. 12). For Sand 1, high values of amplitude (> 62) indicate gas accumulation in the area between faults F1 and F4, and less prominently in some downthrown regions of faults F4 and F6. Note, however, the difficulty in identifying the precise location of the gas-water contact using amplitude distribution in the central area of the map bounded by faults F1 and F2. For Sand 2, its poor expression on seismic data results in a lack of any significant hydrocarbon induced amplitude anomaly. In contrast, the areal acoustic impedance extractions of Fig. 9 are

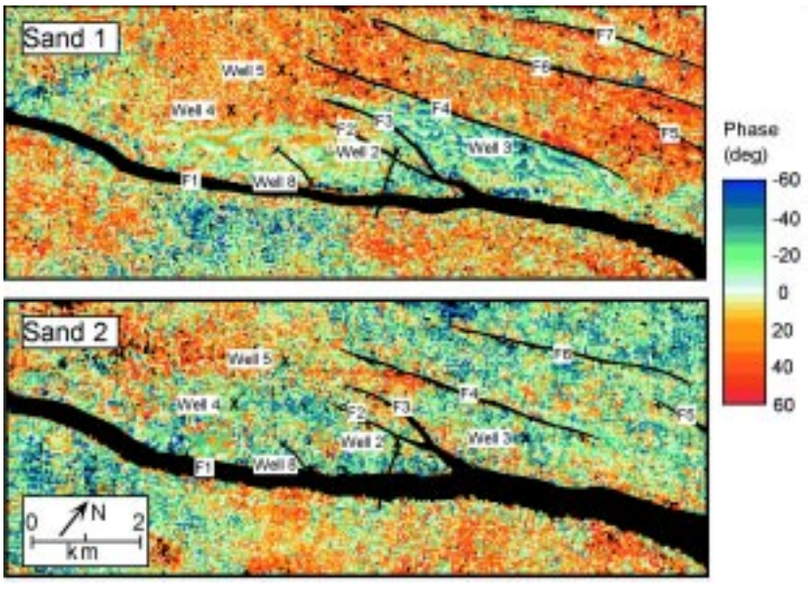

Figure 13 Extracted average instantaneous phase maps for Sand 1 and Sand 2. Symbols as in Fig. 1.

able to not only identify the gas-water contacts for both sands in the central area of the field, but are also able to provide indications of best reservoir quality and higher hydrocarbon saturations as areas having lowest impedance.

Extractions of average instantaneous phase over a 20-ms window centred about the interpreted horizons are shown in Fig. 13 for each sand. The reversal of polarity induced by hydrocarbon occurrence is most obvious on either side of fault F4 for Sand 1: the downthrown area of fault F4 is largely water filled and corresponds to a phase expression of 60°, whereas its footwall area is gas filled and results in a 180° reversal in polarity. For Sand 2, negative polarity is distributed in the central region as well as to the north and north-east. For both sands, it is not possible to isolate the downdip locations of the gas-water contacts solely from considerations of polarity reversal. This uncertainty of identifying the gas water contacts on phase displays also manifests on seismic sections as an inability in picking the precise location of the transition of the waveform amplitude from a peak feature (representing the top of the water filled sand) to a trough feature (representing the top of the gas filled sand). The amplitude and phase extractions, although hydrocarbon indicators in this dataset, are not able, either independently or in combination, to provide the precise locations of the gas water contacts.

Interpretation on acoustic impedance has enabled the delineation of the vertical and lateral extents of gas saturation in both sands to varying degrees of certainty. For Sand 1, wireline crossplots have shown acoustic impedance values beneath an established threshold to relate to gas-sand. Acoustic impedance interpretation is therefore able to demonstrate the extents of a prominent gas reservoir in the central part of the field, and indicate pockets of residual gas accumulation in other areas. For Sand 2, its lower thickness, lower porosity, lower gas saturation, deeper stratigraphic level, poor seismic imaging and differences in petrophysical relationships all combine to create interpretational uncertainty in the resulting acoustic impedance model. In the central area of the field, acoustic impedance interpretations are able to identify the region of gas saturation and locate the gas-water contact, while in the north-east the interpretation becomes ambiguous since the low acoustic impedances may relate to both lithology and fluid effects.

These considerations highlight the limits of usefulness of seismic inverse modelling. Inverse modelling does provide the benefit of layer visualization and possible improvements in resolution, but in order to derive formation characteristics, it is essential that acoustic impedance be calibrated at well locations to fluid and/or lithology. When acoustic impedance is an unequivocal indicator of a particular lithology or fluid, then reservoir properties may be extracted from the impedance volume. Where the type of lithology or type of fluid cannot be isolated based on acoustic impedance, as for Sand 2, then limitations may be imposed on the practicality of impedance interpretation. Nevertheless, in this case study, acoustic impedance interpretations have provided better indications of hydrocarbon distributions than seismic data has been capable, even for the deeper, poorer quality Sand 2. This study has demonstrated the advantages of acoustic impedance interpretation over seismic data interpretation and has illustrated the feasibility, in this field, of using acoustic impedance as a hydrocarbon indicator for reservoirs above the start of overpressuring, and with less certainty, at overpressured depths. Seismic inverse modelling could therefore constitute an important tool in deciding field development strategy.

Acknowledgements

The authors would like to thank Brunei Shell and the Petroleum Unit, Brunei Darussalam for provision of data and for permission to publish the results. Acknowledgements also to Landmark Graphics Corporation for donation of software to the Department of Petroleum Geoscience, University of Brunei Darussalam, through their Strategic University Alliance Agreement; and to Hampson-Russell Software for donation of their inverse modelling software (STRATA) and for their review of this paper.

References

Brown, A.R. [1996] *Interpretation of three-dimensional seismic data*. AAPG memoir 42, 4th edn.

Burge, D.W. and Neff, D.B. [1998] Well based seismic lithology inversion for porosity and pay-thickness mapping. *The Leading Edge* **February**, 166–171.

Duboz, P., Lafet, Y. and Mougenot, D. [1998] Moving to a layered impedance cube: advantages of 3D stratigraphic inversion. *First Break* **16**(9), 311–318.

James, D.M.D. [1984] *The geology and hydrocarbon resources of Negara Brunei Darussalam*, Brunei Museum.

Latimer, R.B., Davison, R. and van Riel, P. [2000] An interpreter's guide to understanding and working with seismic-derived acoustic impedance data. *Leading Edge* **19**(3), 242–256.

Ruijtenberg, P.A., Buchanan, R. and Marke, P. [1990] Three-dimensional data improve reservoir mapping, *Journal of Petroleum Technology* 22–25, 59–61.

Sandal, S.T. [1996] *The geology and hydrocarbon resources of Negara Brunei Darussalam*. 1996 Revision. Brunei Museum.

MS submitted October 2000, accepted March 2000